Journal of Materials Chemistry A

Accepted Manuscript

ROYAL SOCIETY OF CHEMISTRY

www.rsc.org/materialsA

Journal Name

ARTICLE

One-Step Electrochemical Synthesis of Tunable Nitrogen-Doped Graphene

Received 00th January 20xx,
Accepted 00th January 20xx

DOI: 10.1039/x0xx00000x

www.rsc.org/

Fengliu Lou,[a] Marthe Emelie Melandsø Buan,[a] Navaneethan Muthuswamy,[a] John Charles Walmsley,[b, c] Magnus Rønning[a] and De Chen*[a]

A one-step electrochemical approach for the production of tunable nitrogen-doped graphene has been developed in this work. The simultaneous production and nitrogen incorporation of graphene is realized by electrochemical exfoliation of graphite in an aqueous electrolyte containing $(NH_4)_2SO_4$ and $NH_3 \bullet H_2O$, which serve as exfoliating agent and nitrogen source, respectively. Both nitrogen contents and nitrogen bonding configurations can be manipulated by tuning the exfoliation conditions. The mechanism of nitrogen doping is proposed, based on analysis of the released gas from graphite electrode, partially exfoliated graphite and graphene obtained. This green, efficient, low cost and scalable method provides a possible way for the large scale production of high-quality nitrogen-doped graphene. The nitrogen-doped graphene obtained is evaluated as a catalyst for oxygen reduction reaction. It is demonstrated to be among the best nitrogen-doped graphene-based catalysts for oxygen reduction reaction, even though the preparation process is extremely facile. Significantly, Al-air battery is assembled, for the first time, by utilizing nitrogen-doped graphene as cathode catalyst in this work. It can deliver a high specific capacity of 619 mAh g_{Al}^{-1}, corresponding to a specific energy of 817 Wh kg_{Al}^{-1}, which is on par with or better than Al-air battery based on metal catalysts.

Introduction

Graphene, a two dimensional monolayer of sp^2-hybrided carbon sheet, has received increasing attention due to its fascinating properties, such as huge specific surface area, high chemical stability, excellent thermal and electrical conductivity, great mechanical strength and ultrahigh electron mobility.[1-3] It has been explored for many potential applications, especially for oxygen reduction reaction (ORR)[4-8] which is of significance for metal-air batteries and fuel cells.[9] However, high-quality graphene exhibits zero band gap characteristics, which weakens its catalytic activity.[10,11] Fortunately, doping with heteroatoms has been demonstrated as a successful way to manipulate the electronic structure, tune the band gap and increase the number of active sites, thus enhancing the catalytic activity.[10]

Nitrogen-doped graphene has been the most intensively investigated doping system because nitrogen has a comparable atomic size with carbon and contains five valence electrons for bonding with carbon atoms.[10,12] Generally, nitrogen-doped graphene has been prepared either through a top-down approach, to produce graphene or graphene oxide from graphite followed by a post-treatment, such as thermal,[13] plasma,[14] electrochemical[15] or hydrothermal processes,[16] or through a bottom-up approach, such as chemical vapor deposition,[4] arc discharge[17] or solvothermal processes.[18] For the top-down approaches, graphene oxide usually needs to be prepared in a first step, which presents the inherent disadvantages of explosion risk, release of hazardous gas, huge energy consumption and discharge of polluted water.[19] For the bottom-up approaches, harsh reaction conditions are usually required in addition to the low productivity. Recently, electrochemical exfoliation of graphite for the production of graphene has attracted considerable attention, due to the high productivity and simplicity.[20,21] Zhao and coworkers reported the use of ethylammonium nitrate or ammonium nitrate as electrolyte for the production of nitrogen-doped graphene by electrochemical exfoliation.[22,23] However, the unsatisfied quality of nitrogen-doped graphene obtained, in terms of doping level (1.3 at%) and flake thickness (9 layers), limits the electrocatalytic activity.[22] Therefore, the development of a green, simple and cost-effective approach for the scalable production of high-quality nitrogen-doped graphene with a significantly improved electrochemical performance is still highly desirable.

In this work, a one-step electrochemical approach for the production of high-quality nitrogen-doped graphene has been developed. Both nitrogen contents and nitrogen bonding

[a] Department of Chemical Engineering, Norwegian University of Science and Technology, Sem Sælands vei 4, N-7491 Trondheim, Norway. E-mail: de.chen@ntnu.no
[b] Department of Physics, Norwegian University of Science and Technology, Høgskoleringen 5, N-7491 Trondheim, Norway
[c] SINTEF Materials and Chemistry, Høgskoleringen 5, N-7465 Trondheim, Norway
† Footnotes relating to the title and/or authors should appear here.
Electronic Supplementary Information (ESI) available: [details of any supplementary information available should be included here]. See DOI: 10.1039/x0xx00000x

configurations can be manipulated by tuning the exfoliation conditions. This green, efficient, low cost and scalable method provides a possible way for the fast synthesis of high-quality nitrogen-doped graphene which can facilitate the fundamental study of doped graphene and also supplies a potential approach for the large scale production of high-quality nitrogen-doped graphene. The nitrogen-doped graphene obtained is demonstrated to be among the best nitrogen-doped graphene-based catalysts for oxygen reduction reaction, even though the preparation process is extremely facile. Significantly, high performance Al-air battery is assembled, for the first time, by utilizing nitrogen-doped graphene as cathode catalyst in this work.

Experimental Section

Preparation of nitrogen-doped graphene

Nitrogen-doped graphene was produced via electrochemical exfoliation of graphite by utilizing an aqueous solution of $(NH_4)_2SO_4$ (Fluka, ≥99%) and $NH_3•H_2O$ (Sigma-Aldrich, 28-30%) as electrolyte at 25 or 60 ^oC. The exfoliation temperature was controlled by employing a thermostatic water bath. Graphite foil (Alfa Aesar, 97%) and Pt mesh were employed as working and counter electrode, respectively, with a distance of 2 cm. A positive voltage of 4, 7.5 or 15 V was applied on the working electrode through a power supplier (Delta Elektronika). The exfoliated graphene sheets were collected with a polyvinylidene fluoride membrane filter (Millipore, pore size 220 nm) and washed with distilled water by vacuum filtration. Afterwards, the obtained materials were dispersed into 96% ethanol by sonication for 60 min. The suspension was subjected to centrifugation at 2500 rpm for 20 min to remove the unexfoliated graphite. The centrifuged suspension was used for further characterization and application. Additionally, a reference undoped graphene sample was prepared with the same procedure but without $NH_3•H_2O$ in the electrolyte solution during electrochemical exfoliation.

Material characterization

Graphene suspensions were coated on freshly cleaved mica and silicon wafer by spin coating for atomic force microscopy (AFM) and Raman characterizations, respectively. The AFM images were obtained on Veeco Metrology-diMultimode V system by using tapping mode. Raman spectra were collected on a Renishaw InVia Reflex Spectrometer System by using VIS excitation at 532 nm. The microstructure of the graphene was characterized by employing a high-resolution transmission electron microscope (TEM) with a field emission gun (JEOL JEM 2010F) at an acceleration voltage of 80 kV. FTIR spectra were recorded on a Nicolet™ iS™50 FTIR spectrometer in the 400–4000 cm^{-1} wave number range. 128 scans were taken at a resolution of 4 cm^{-1}. X-ray photoelectron spectroscopy (XPS) analyses were carried out using a Kratos Axis Ultra DLD spectrometer with a monochromatic AlK_α radiation (hv=1486.58 eV). High-resolution spectra were collected at a pass energy of 20 eV. The graphene samples were dried at 120 ^oC for 24 hours under vacuum before XPS test to minimize the physically absorbed NH_3 and water. The deconvolution of the C 1s, O 1s and N 1s peaks was performed by using XPS Peak 4.0 software with Shirley background and least-squared optimization algorithm. Temperature programmed desorption measurements were performed on a STA 449 C analyzer (Netzsch, Germany) connected to a mass spectrometer (MS, QMS 403) at a heating rate of 10 $^oC\ min^{-1}$ between 50 and 600 ^oC under argon atmosphere.

Oxygen reduction reaction

The electrochemical oxygen reduction properties of graphene were evaluated by using a three-electrode system at room-temperature. Pt wire and Ag/AgCl electrode filled with 3.5 M KCl aqueous solution were employed as counter and reference electrode, respectively. The electrolyte was 0.1 M KOH aqueous solution, which was purged with argon or oxygen for at least 30 min prior to the electrochemical test. The catalyst ink was prepared by dispersing 2 mg graphene into 2 ml ethanol solution containing 8 µl of 5 wt% Nafion (Alfa Aesar, D520 dispersion) by sonication for 60 min. 20 µl of the obtained catalyst ink was dip coated onto the glassy carbon electrode (5 mm diameter) and dried at room-temperature overnight. The cyclic voltammetry and rotating disk electrode measurements were performed using a Princeton VersaSTAT potentiostat analyzer (Princeton Applied Research). For comparison, a commercially available catalyst of 20 wt% platinum on Vulcan carbon black (Pt/C from E-tek) was also evaluated. The Pt/C coated glassy carbon electrode was prepared according to the same procedure described above.

The Koutecky-Levich equation was employed to calculate the electron transfer number:[47,55]

$$\frac{1}{J}=\frac{1}{J_L}+\frac{1}{J_K}=\frac{1}{B\omega^{1/2}}+\frac{1}{J_K} \quad (1)$$

$$B=0.2nFC_0(\mathrm{D}_0)^{2/3}\nu^{-1/6} \quad (2)$$

where J is the measured current density, J_L is the diffusion limiting current density, J_K is the kinetic limiting current density, ω is the rotating speed in rpm, F is the Faraday constant (96 485 C mol^{-1}), D_0 is the diffusion coefficient of oxygen in 0.1 M KOH (1.9×10^{-5} $cm^2\ s^{-1}$), ν is the kinetic viscosity (0.01 $cm^2\ s^{-1}$), and C_0 is the buck concentration of oxygen (1.2×10^{-3} mol L^{-1}).

Al-air battery

A home-made Al-air battery was assembled to evaluate the catalytic performance of graphene in an Al-air single cell battery. The air electrode was fabricated by uniformly coating graphene ink onto carbon paper (AvCarb P50T, Fuel Cell Store) with an active electrode area of 2.5 cm^2. The graphene ink was prepared by dispersing graphene into Nafion contained isopropanol solution at a concentration of 10 mg ml^{-1}. The catalyst ink, containing a graphene to Nafion weight ratio of 5:1, was then air brush sprayed onto carbon paper and then dried at 80 ^oC for 2 hours. The graphene mass loading was 1 mg cm^{-2}. Al foil (99.45%, Alfa Aesar) and 4 M KOH in 80%

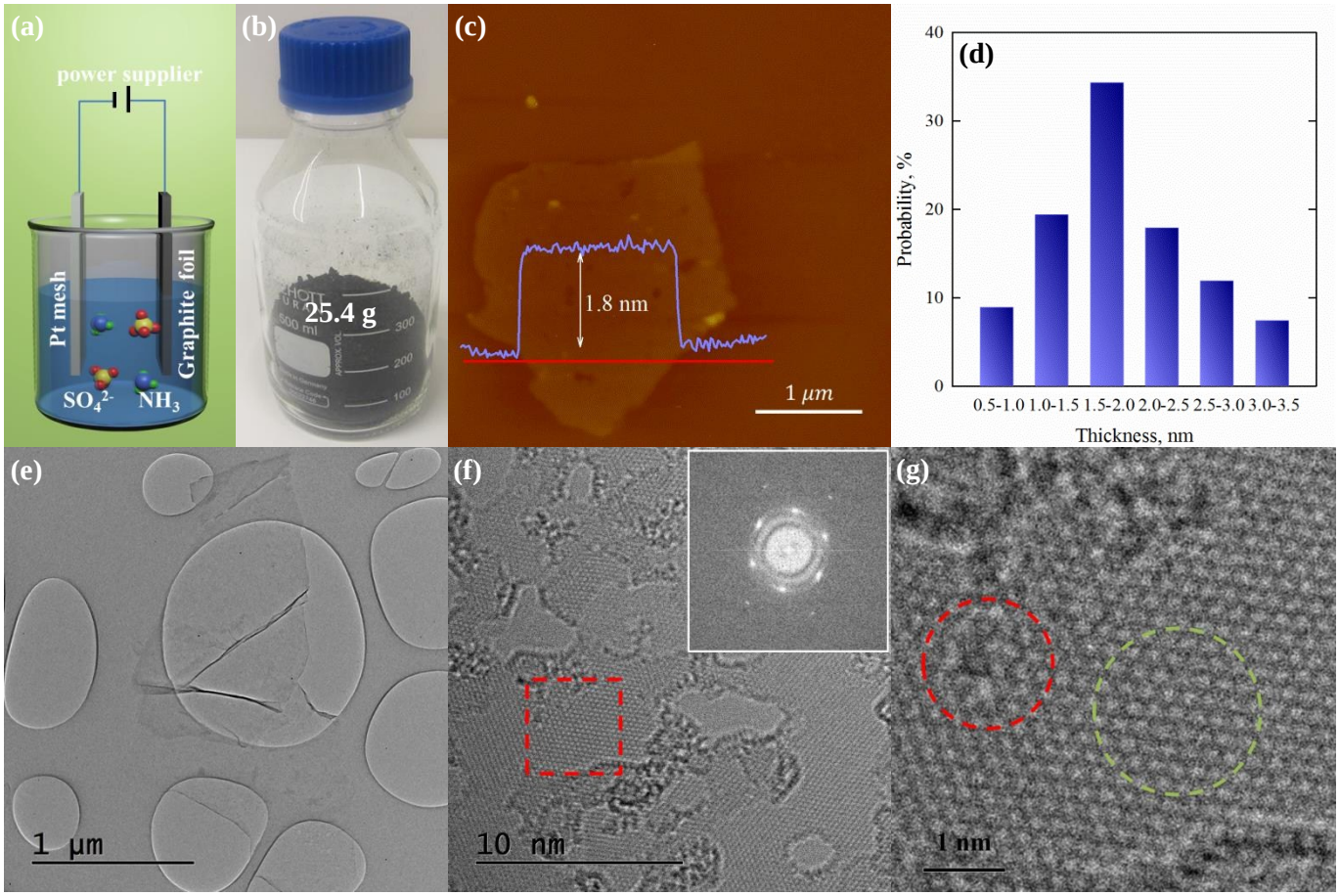

Fig. 1 Electrochemical production of nitrogen-doped graphene. a) Schematic illustration of the electrochemical preparation of N-Graphene. b) Photograph of 25.4 g N-Graphene powder. c) Typical AFM image of N-Graphene with a height profile (blue curve) taken along the red line. The sample was prepared by spin coating of N-Graphene suspension on freshly cleaved mica. d) The thickness distribution of about 80 pieces of N-Graphene sheets obtained from the AFM height profile. e) Typical bright field TEM image of N-Graphene. f) High-resolution TEM image of N-Graphene. The inset is a FFT of the whole image. g) Enlarged image of the red box in panel f.

ethanol were used as anode and electrolyte respectively. The as-assembled Al-air battery was tested by galvanostatic discharge at a current density of 1 mA cm^{-2}.

Results and Discussion

Electrochemical production of nitrogen-doped graphene

The one-step production of nitrogen-doped graphene was realized by electrochemical exfoliation of graphite in a mixed aqueous electrolyte containing $NH_3•H_2O$ and $(NH_4)_2SO_4$ (Fig. 1a). The selection of $NH_3•H_2O$ and $(NH_4)_2SO_4$ aqueous solution as electrolyte was based on the following considerations. Firstly, $NH_3•H_2O$ has been widely used as nitrogen source for the synthesis of nitrogen-doped graphene[5,7] and highly nitrogen-doped carbon particles has been synthesized by electrochemical exfoliation of graphite in $NH_3•H_2O$ containing electrolyte.[24] Secondly, SO_4^{2-} has been demonstrated as an efficient exfoliating agent for the preparation of graphene.[20,21] Finally, water is a kind of green and cost-effective solvent. Unless noted otherwise, all results reported are presented from N-Graphene, which was obtained by applying 7.5 V voltage at room temperature (25 °C) with 5 M $NH_3•H_2O$ and 1 M $(NH_4)_2SO_4$ mixed aqueous solution as electrolyte. In contrast to carbon particles, graphene sheets were successfully obtained after introducing SO_4^{2-} into $NH_3•H_2O$ containing electrolyte (Fig. 1c), demonstrating the strong exfoliating ability of SO_4^{2-} toward graphite. The thickness distribution of about 80 pieces of N-Graphene sheets obtained from the atomic force microscope (AFM) height profile is presented in Fig. 1d. N-Graphene sheets exhibit an average thickness of 1.9 nm and a maximum thickness of 3.5 nm. Thus, N-Graphene is typical 3-5 layer graphene, but single layer graphene also exists which accounts for about 9 %. As shown in a typical transmission electron microscope (TEM) image of a single flake (Fig. 1e), N-Graphene has weak and uniform contrast, relative to the carbon support film, indicating again a low and constant thickness. The lattice resolution image of Fig. 1f shows a region of N-Graphene that is monolayer as evidenced by its fast Fourier transform (FFT).[25] As shown in the enlarged image (Fig. 1g), both defect free hexagonal arrangement of carbon

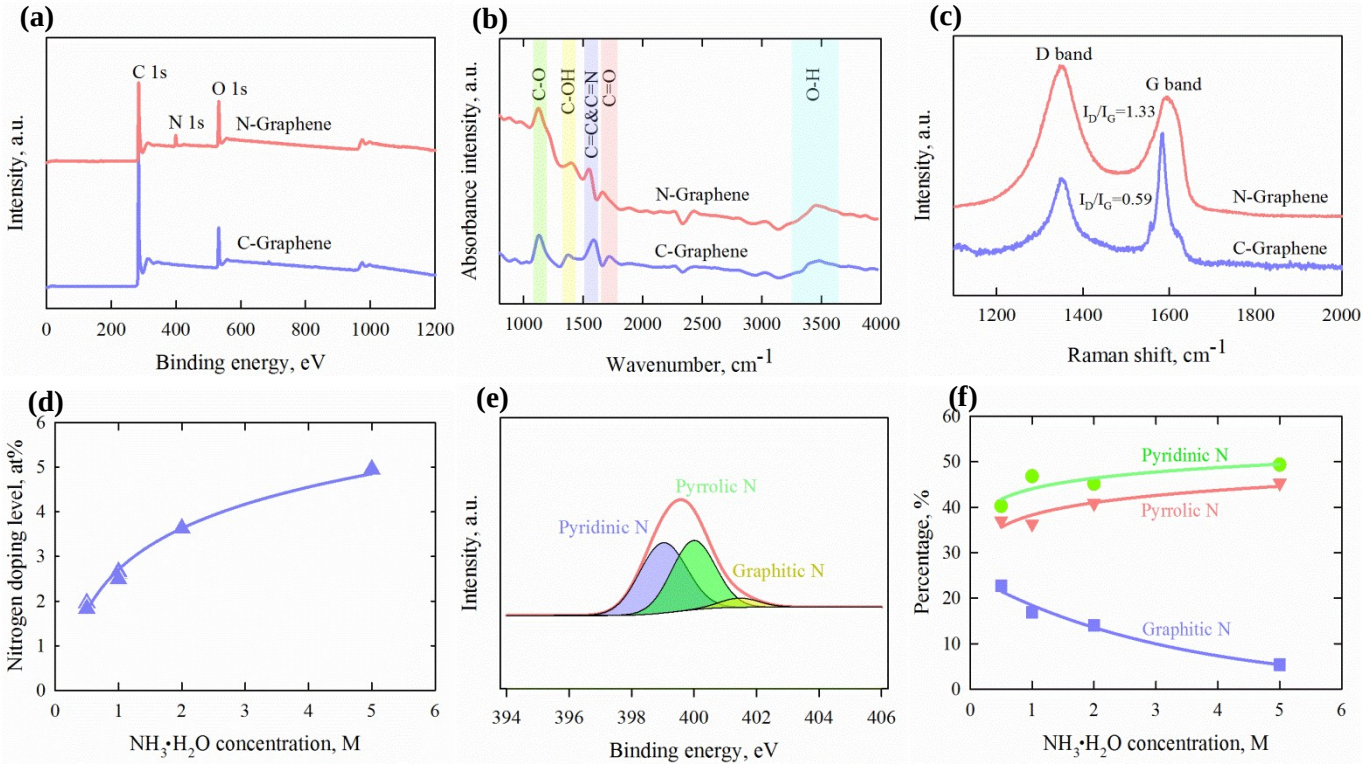

Fig. 2 Evidence of successful nitrogen doping and property manipulation. a) XPS survey spectra of C-Graphene and N-Graphene. FTIR spectra (b) and Raman spectra (c) of C-Graphene and N-Graphene. d) The dependence of nitrogen doping level on the concentration of $NH_3 \bullet H_2O$ in the electrolyte. e) High-resolution N 1s XPS spectrum of N-Graphene. f) The dependence of nitrogen configuration on the concentration of $NH_3 \bullet H_2O$ in the electrolyte.

(labeled by a green circle) and possible nitrogen doping induced defects (labeled by a red circle) can be observed. In order to understand the nitrogen doping mechanism and demonstrate the function of nitrogen doping, a reference sample C-Graphene was prepared by using the same exfoliation conditions as N-Graphene but without $NH_3 \bullet H_2O$ in the electrolyte. C-Graphene shows similar flake size and thickness distribution as N-Graphene (Fig. S1a and b, ESI). However, C-Graphene presents relatively less defects compared with N-Graphene (Fig. S1d, ESI). Therefore, the presence of $NH_3 \bullet H_2O$ in the electrolyte has no obvious effects on the graphene thickness and flake size but increases the number of defects.

X-ray photoelectron spectroscopy (XPS) was carried out to investigate the elemental compositions of graphene obtained. As shown in Fig. 2a, the XPS survey spectrum of C-Graphene only shows the presence of carbon (91.83 at%) and oxygen (8.17 at%), which is consistent with previous report.[21] However, the XPS spectrum of N-Graphene clearly shows the presence of nitrogen (4.95 at%) in addition to carbon (83.40 at%) and oxygen (11.66 at%) (Fig. 2a). The existence of physically absorbed NH_3 on the surface of graphene is inevitable due to its high specific surface area, pore structure and functional group. Thermogravimetric-mass spectrometric analysis was conducted to measure the contribution of physically absorbed NH_3 on the total nitrogen content of obtained N-Graphene (Fig. S2, ESI). An acceptable error of 6.1% was found. Therefore, the nitrogen contents obtained from XPS are reliable. Furthermore, Fourier transform infrared (FTIR) and Raman spectra were acquired to further identify the successful doping of nitrogen into graphene frameworks. The peak at 1585 cm^{-1} for C-Graphene, corresponding to the stretching vibration of C=C bonds, shifts to 1555 cm^{-1} for N-Graphene (Fig. 2b). This is due to the superposition of the vibrations of C=C and C=N bonds, which gives clear evidence of the embedding of nitrogen containing groups in graphene layers.[26] According to Raman spectra (Fig. 2c), the G band of N-Graphene shows an obvious upshift compared with C-Graphene, from 1583 to 1593 cm^{-1}. The upshift of the G band may be due to the presence of dopants or defects which modify the free carrier concentration.[8,27] Additionally, the I_D/I_G ratio of N-Graphene exhibits an obvious increase compared with C-Graphene, from 0.59 to 1.33. The larger I_D/I_G ratio is a result of the structural defects and edge plane exposure caused by nitrogen atom incorporation into the graphene layers.[28] This is consistent with the TEM results. Therefore, nitrogen-doped graphene was successfully synthesized by electrochemical exfoliation of graphite in the mixed aqueous electrolyte of $NH_3 \bullet H_2O$ and $(NH_4)_2SO_4$. However, nitrogen-doped carbon particles[24] and undoped graphene were synthesized by electrochemical exfoliation of graphite in $NH_3 \bullet H_2O$ aqueous electrolyte and $(NH_4)_2SO_4$ aqueous

electrolyte, respectively. Thus, $NH_3•H_2O$ and $(NH_4)_2SO_4$ serves as nitrogen source and exfoliating agent, respectively, during the electrochemical preparation of N-Graphene.

The electrochemical performances of nitrogen-doped graphene depend strongly on its properties, such as nitrogen doping level, oxygen content and nitrogen bonding configuration.[8,10] Therefore, the dependence of graphene properties on the exfoliation conditions was systematically investigated. As presented in Fig. 2d, the nitrogen doping level can be well manipulated in the range of 1-5 at% by controlling the concentration of $NH_3•H_2O$ in the electrolyte (Table S1, ESI). Notably, a high nitrogen doping level of 8.58 at% has been achieved when the exfoliation was performed at 60 ^oC which is 2 times higher than the one obtained at 25 ^oC (Table S2, ESI). This value is also significantly higher than the one obtained by using ammonia nitrate as electrolyte (1.3 at%).[22] However, the concentrations of NH_4^+ and OH^- as well as exfoliation voltage have no clear effect on the nitrogen doping level (Table S1 and S3). Moreover, the oxygen contents exhibit clear dependence on exfoliation voltages (Table S3, ESI). The higher exfoliation voltage results in higher oxygen content. However, exfoliation voltages have almost no effect on nitrogen doping level. This makes the investigation of the effect of oxygen content on the electrochemical performance of nitrogen-doped graphene possible. High-resolution XPS spectra were collected to investigate the nitrogen bonding configurations. The N 1s spectrum can be deconvoluted into three peaks: peak I (398.1-399.3 eV), pyridinic nitrogen; peak II (399.8-401.2 eV), pyrrolic nitrogen; and peak III (401.1-402.7 eV), graphitic nitrogen.[8,29] According to Fig. 2e, pyridinic (49.3 %) and pyrrolic (45.3 %) nitrogen are the dominating nitrogen configurations in N-Graphene (Table S5, ESI). In addition, the nitrogen configurations can be tuned by controlling the concentration of $NH_3•H_2O$ in the electrolyte as well (Fig. 2f). Therefore, both nitrogen doping levels and bonding configurations can be tuned by controlling the exfoliation conditions, which indicates the flexibility of this method.

The graphene yields were calculated by dividing graphene weight by the total weight of graphene and unexfoliated graphite. The yields of N-Graphene and C-Graphene are 34 wt% and 41 wt%, respectively, indicating that the presence of $NH_3•H_2O$ has little effect on the yields. Additionally, N-Graphene can be easily dispersed in water, without any precipitation for several days, and can be stable for several months in ethanol (Fig. S7, ESI). However, C-Graphene shows very poor dispersion properties, forms flocs in water and ethanol, and is only stable in N-methyl-2-pyrrolidone. The greater hydrophilicity of N-Graphene, compared with C-Graphene makes the subsequent treatment easier. Moreover, 25.4 g N-Graphene can be easily produced in the laboratory (Fig. 1b), which demonstrates the electrochemical exfoliation of graphite is an easily scalable method for the production of nitrogen-doped graphene.

Mechanism of nitrogen-doped graphene formation

In an aqueous solution, $NH_3•H_2O$, NH_3 and NH_4^+ are in equilibrium according to Equation 3:

$$NH_3 \bullet H_2O \leftrightarrow NH_3 + H_2O \leftrightarrow NH_4^+ + OH^- \quad (3)$$

The predominant nitrogen containing species is NH_4^+ in 1M $(NH_4)_2SO_4$ aqueous electrolyte (used for the preparation of C-Graphene) (Table S1). The electrochemical oxidation of NH_4^+ is direct electrochemical decomposition to form N_2 without adsorption step.[30-32]

$$2NH_4^+ \rightarrow N_2 + 8H^+ + 6e^- \quad (4)$$

Therefore, it is impossible to synthesize nitrogen-doped graphene by electrochemical oxidation of NH_4^+ because no nitrogen containing species is adsorbed on the graphite electrode surface. However, both NH_3 and NH_4^+ are imorptant nitrogen containing species in 5 M $NH_3•H_2O$ and 1 M $(NH_4)_2SO_4$ mixed aqueous electrolyte (used for the preparation of N-Graphene) (Table S1). The electrochemical oxidation of NH_3 involves dehydrogenation of adsorbed NH_3 and formation of N_2 according to Equation 5:[32-34]

$$NH_{3(aq)} \rightarrow NH_{3,ads} \quad (5a)$$

$$NH_{3,ads} \rightarrow NH_{2,ads} + H^+ + e^- \quad (5b)$$

$$NH_{2,ads} \rightarrow NH_{ads} + H^+ + e^- \quad (5c)$$

$$NH_{ads} \rightarrow N_{ads} + H^+ + e^- \quad (5d)$$

$$NH_{x,ads} + NH_{y,ads} \rightarrow N_2 + (x+y)H^+ + (x+y)e^- \quad (5e)$$

Additionally, NO_x can be formed when oxygen containing species exist on the electrode surface.[32]

In order to investigate the mechanism of nitrogen doping, the gases released from the graphite electrodes during electrochemical exfoliation, the partially exfoliated graphite electrodes, and the graphene obtained were analyzed. Firstly, the gases released from the graphite electrode was carefully collected with the help of a Calibrated Instruments gas sampling bag and analyzed by using mass spectrometer. H_2O (m/z=18), N_2 and/or CO (m/z=28), O_2 (m/z=32), and CO_2 (m/z=44) were detected from the gasese collected during the preparation of C-Graphene (elctrolyte: 1 M $(NH_4)_2SO_4$) (Fig. 3a). H_2O originates from the steam, while N_2 and O_2 can be attributed to the decomposition of NH_4^+ and H_2O, respectively.[32,35] CO and CO_2 are due to the electrochemical oxidation of graphite electrodes.[21] In addition to these species, NO_x (m/z=30, 46) was also detected from the gases collected during the preparation of N-Graphene (electrolyte: 5 M $NH_3•H_2O$ and 1 M $(NH_4)_2SO_4$) (Fig. 3b). This can be attributed to the reaction between N_{ads} generated from dehydrogenation of adsorbed NH_3 and oxygen containing groups on the electrode surface.[32] The absence of H_2 (m/z=2) and SO_2 (m/z=64) in the released gases might be due to the formation of H_2O and the high solubility of SO_2 in water[36], respectively. Additionally, the partially exfoliated graphite electrodes were analyzed by temperature programmed desorption to gain further insight into the intermediates of NH_3 and NH_4^+ electrochemcial oxidation. The mass spectra of H_2 (m/z=2), NH_3 (m/z=17) and N_2 (m/z=28) are featureless (Fig. 3c), which indicates none of them were deteted from partially exfoliated

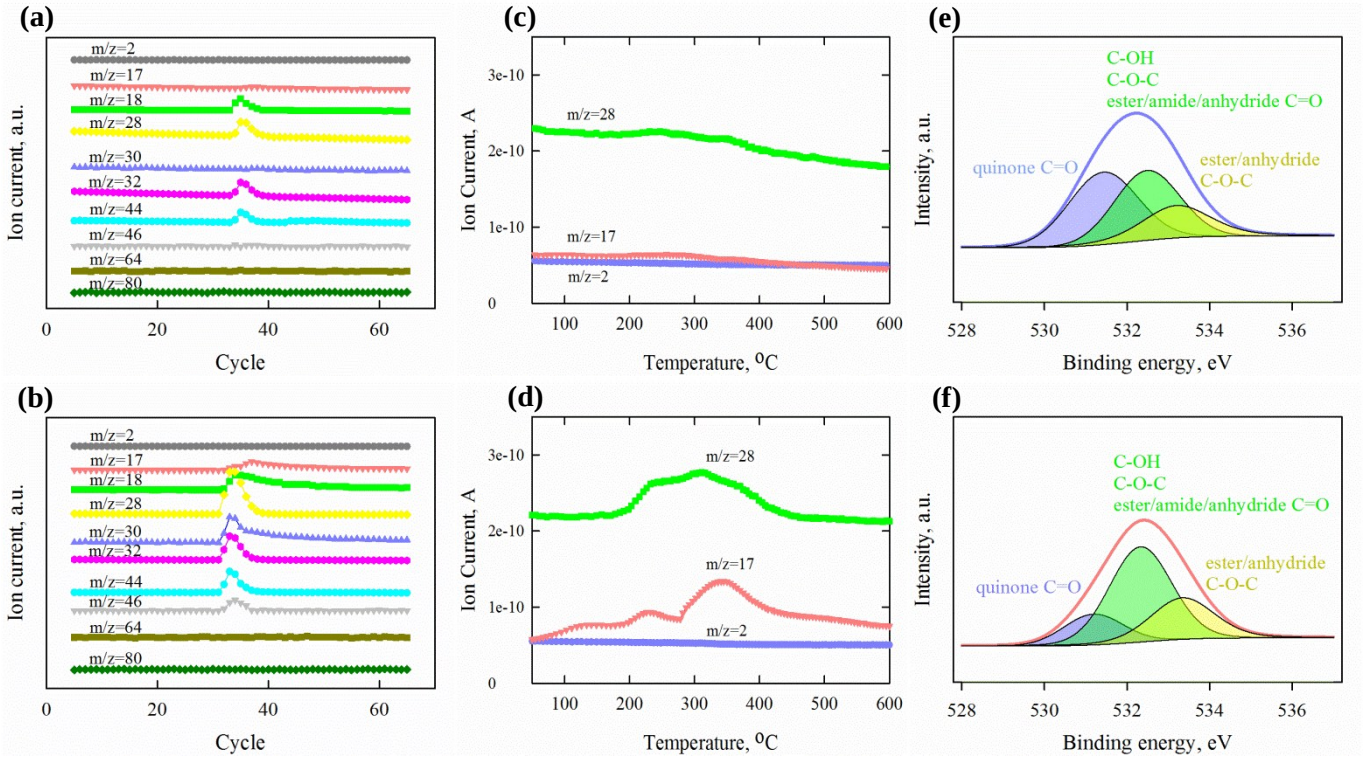

Fig. 3 Mechanism of nitrogen doping. Mass spectra of gases released from the graphite electrodes during electrochemical preparation of C-Graphene (a) and N-Graphene (b). The gases were carefully collected with the help of a specially designed funnel and transferred using a Calibrated Instruments gas sampling bag. Temperature programmed desorption spectra of gases released from the partially exfoliated graphite electrodes used for the preparation of C-Graphene (c) and N-Graphene (d). High-resolution O 1s XPS spectra of C-Graphene (e) and N-Graphene (f).

graphite electrodes used for the preparation of C-Graphene. However, both NH_3 (m/z=17) and N_2 (m/z=28) were detected from partially exfoliated graphite electrodes used for the preparation of N-Graphene (Fig. 3d). The synchronous evolution of NH_3 (m/z=17) and N_2 (m/z=28) at relatively high temperature indicates that they are produced from the adsorbed intermediate $NH_{x,ads}$ according to the following reaction:

$$NH_{x,ads} \rightarrow \frac{3-x}{6} N_2 + \frac{x}{3} NH_3 \quad (6)$$

Therefore, the existance of $NH_{x,ads}$ on the graphite electrode surface during the preparation of N-Graphene was fully confirmed and this is entirely consistent with the theories mentioned previously. Nitrogen atoms are genreally incorporated into graphene lattices through the interaction between nitrogen and oxygen containing groups followed by rearrangement.[16,37] Therefore, the oxygen binding configurations were analyzed with the help of high-resolution XPS. The deconvolution of O 1s spectra gives three peaks: peak I (531.0–531.9 eV), carbonyl oxygen of quinones; peak II (532.3–532.8 eV), carbonyl oxygen atoms in esters, amides, anhydrides and oxygen atoms in hydroxyls or ethers; peak III (533.1–533.8 eV), the ether oxygen atoms in esters and anhydrides (Fig. 3e and f).[38,39] The total oxygen contents are 8.17 and 11.66 at% for C-Graphene and N-Graphene, respectively. However, the quinone groups are 3.4 and 1.9 at% for C-Graphene and N-Graphene, respectively (Table S6, ESI). Therefore, the total oxygen content increases after adding $NH_3 \bullet H_2O$ into the electrolyte but the amount of quinone group decreases.

A possible mechanism of nitrogen-doped graphene formation is proposed based on the results in this work and the published literatures.[35,40,41] In the beginning, anodic oxidation of water produced hydroxyl (·OH) and oxygen (·O) radicals.[35,40]

$$H_2O \xrightarrow{-e^-} \bullet OH + H^+ \xrightarrow{-e^-} \bullet O + H^+ \longrightarrow \frac{1}{2} O_2 \quad (7)$$

The hydroxylation or oxidation of graphite by these radicals results in the corrosion at edge sites, grain boundaries, or defect sites and the introduction of oxygen containing groups, such as hydroxyl and carboxyl group.[40] Thus, the oxidation of graphite edge planes by radicals opens up the edge sheets, facilitating the intercalation of SO_4^{2-}.[35] Solvent H_2O can be co-intercalated into graphite electrode during this stage.[21]

$$[C_n] + [SO_4^{2-}] + xH_2O = [C_n^{2+} SO_4^{2-} \bullet xH_2O] + 2e^- \quad (8)$$

Meanwhile, the oxygen containing groups on the graphite electrode, such as quinone groups, can interact with the NH_3 oxidation intermediate, such as $NH_{x,ads}$,[42] which results in the incorporation of nitrogen atom into the graphite lattice. This

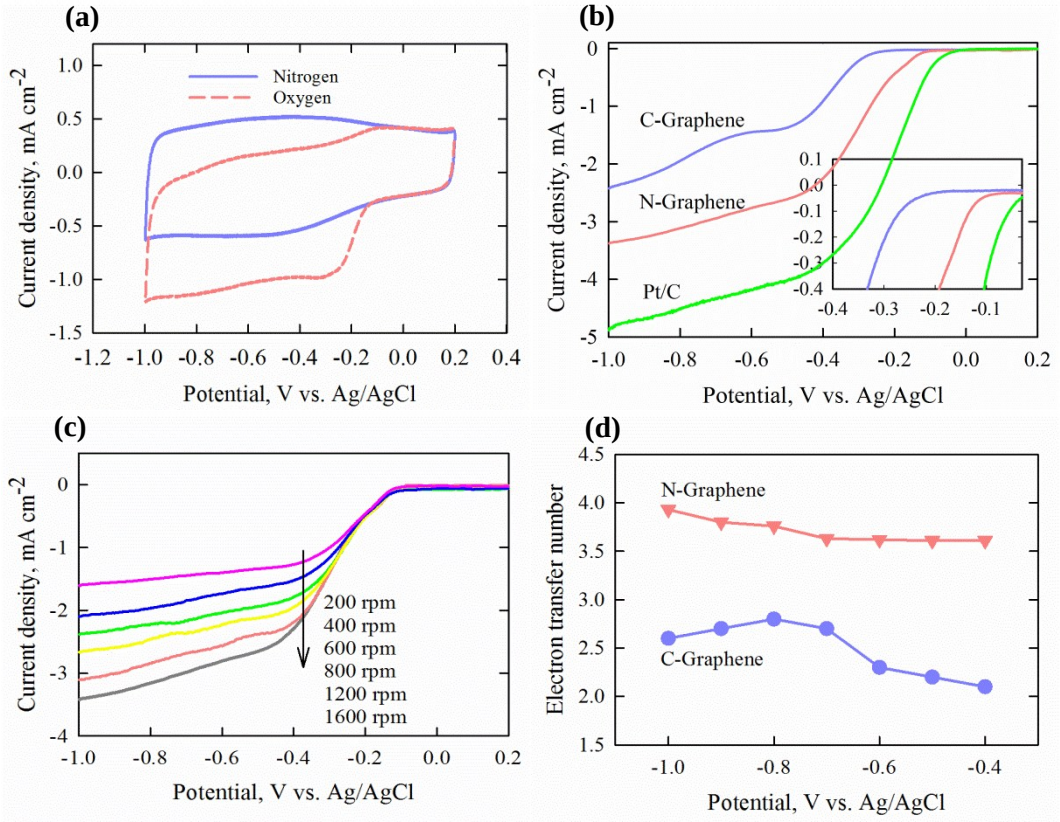

Fig. 4 Electrocatalytic activity of N-Graphene as a catalyst for ORR. a) Cyclic voltammograms of N-Graphene in an argon or oxygen saturated 0.1 M KOH aqueous solution at a scan rate of 100 mV s^{-1}. b) RDE voltammograms of C-Graphene and N-Graphene in oxygen saturated 0.1 M KOH aqueous solution at a scan rate of 10 mV s^{-1} and a rotation rate of 1600 rpm. The inset shows the enlarged high-potential region of the plots. c) RDE voltammograms of N-Graphene in oxygen saturated 0.1 M KOH aqueous solution at a scan rate of 10 mV s^{-1} and various rotating rates. d) The electron transfer number of C-Graphene and N-Graphene as a function of potential.

proposal is also consistent with the finding of Li and coworkers.[43] These nitrogen atoms probably exist on the edges, in the form of pyridinic and pyrrolic nitrogen, at the initial stage of exfoliation, and then transform to graphitic nitrogen afterwards.[13] Finally, the reduction of SO_4^{2-} anions and self-oxidation of H_2O generate gaseous species such as SO_2 and O_2, as evidenced by the vigorous gas evolution during the exfoliation process. The generated gaseous species can produce high pressure which results in the exfoliation of graphite electrode.[21] Thus, nitrogen-doped graphene was produced and released into the electrolyte.

Therefore, high-quality nitrogen-doped graphene with tunable nitrogen contents and bonding configurations has been successfully synthesized by one-step electrochemical exfoliation of graphite in a mixed aqueous electrolyte containing $NH_3•H_2O$ and $(NH_4)_2SO_4$. In the electrolyte system, $NH_3•H_2O$ serves as nitrogen source, while SO_4^{2-} is responsible for graphite exfoliation. The presence of $NH_3•H_2O$ in the electrolyte is essential for the successful synthesis of nitrogen-doped graphene because NH_3 can be adsorbed on the electrode surface during NH_3 oxidation. Recently, boron-doped graphene quantum dots have been prepared by electrochemical exfoliation of graphite.[44,45] We believe boron-doped graphene can be synthesized in the same way by adding SO_4^{2-} into the electrolyte to enhance the graphite exfoliation.

Electrocatalytic activity of N-Graphene as a catalyst for ORR

In order to demonstrate the nitrogen doping functions and explore the potential applications, N-Graphene was evaluated as a catalyst for ORR. Cyclic voltammetry (CV) and rotating disk electrode (RDE) measurements were carried out in 0.1 M KOH to assess the ORR activity. C-Graphene and 20 wt% platinum on Vulcan carbon black (Pt/C) were measured as references. In argon saturated 0.1 M KOH solution, a pure capacitive background is observed for N-Graphene (Fig. 4a). The introduction of oxygen leads to a well-defined reduction peak at -0.29 V corresponding to ORR, which clearly indicates the catalytic activity of N-Graphene. The onset potential for the ORR is an important criterion to evaluate the electrocatalyst activity. As shown in Fig. 4b, the N-Graphene sample presents a positively shifted onset potential at -0.08V, compared with -0.18 V for C-Graphene, which can be attributed to the effect of nitrogen doping.[5,13,46] In addition, the reduction current for ORR catalyzed by N-Graphene is much larger compared with C-Graphene (Fig. 4b). Both the positive shift of onset potential and the enhanced reduction current for ORR on N-Graphene

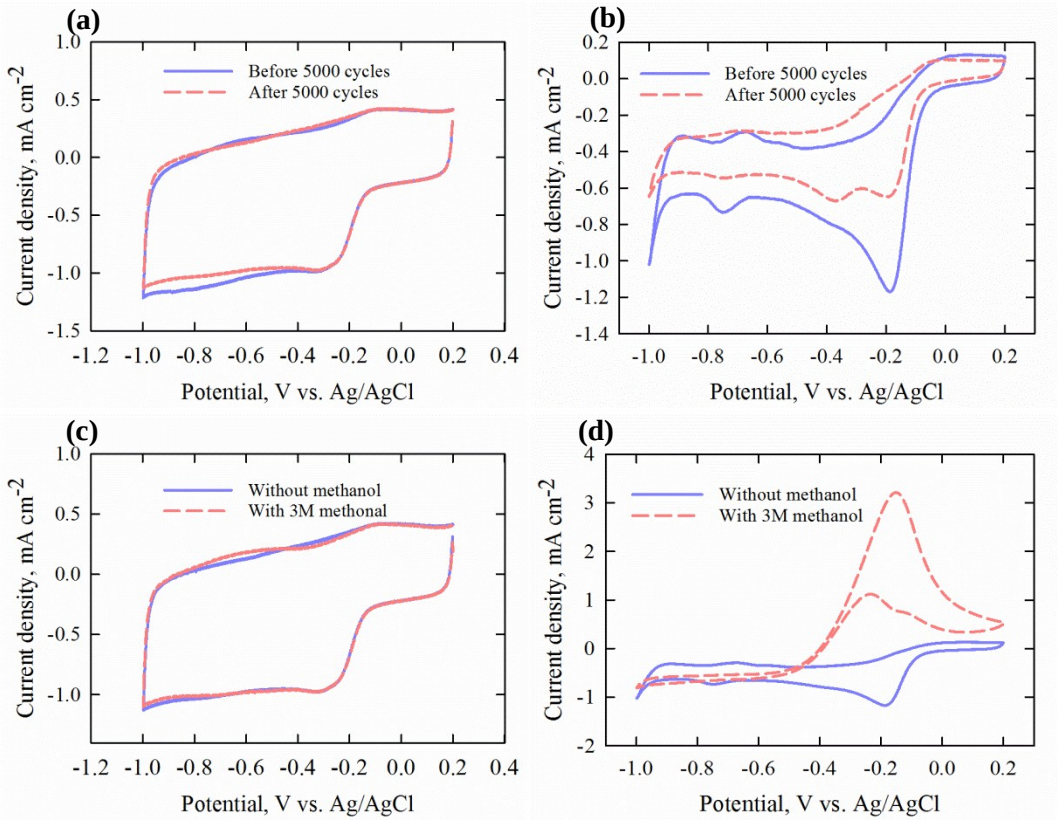

Fig. 5 Durability and methanol tolerance tests of N-Graphene as a catalyst for ORR. Cyclic voltammograms of N-Graphene (a) and Pt/C (b) before and after durability test (5000 cycles in oxygen saturated 0.1 M KOH aqueous solution at a scan rate of 100 mV s^{-1}) at a scan rate of 100 mV s^{-1}. Cyclic voltammograms of N-Graphene (c) and Pt/C (d) in oxygen saturated 0.1 M KOH aqueous solution with and without 3 M methanol at a scan rate of 100 mV s^{-1}.

demonstrate that N-Graphene possesses much higher electrocatalytic activity toward ORR than C-Graphene. However, the catalytic activity of N-Graphene is still inferior to that of Pt/C (Fig. 4b).

The ORR on a catalyst surface can either produce hydrogen peroxide as the product through a two electron process, or produce water through a four electron process.[13] The four electron pathway is obviously more efficient and favorable.[13] Therefore, the electron transfer number per oxygen molecule was determined from RDE measurements (Fig. 4c and d, and Fig. S8 in ESI). The RDE voltammograms of C-Graphene and N-Graphene were recorded at different rotating rates from 200 to 1600 rpm between 0.2 and -1.0 V. The Koutecky-Levich plots of both samples display good linearity (Fig. S8b and c). From the fitting results as shown in Fig. 4d, the ORR on C-Graphene is dominated by a two electron process with hydrogen peroxide as the main product. The electron transfer number varies from 2.1 to 2.8 in the potential range from -0.4 to -1.0 V (Fig. 4d). However, the ORR on N-Graphene is dominated by an efficient four electron process with water as the main product and the electron transfer number varies from 3.6 to 3.9 in the same potential range (Fig. 4d). This indicates that N-Graphene is a more efficient electrocatalyst than C-Graphene towards ORR. According to Table S7 (ESI), N-Graphene is among the best nitrogen-doped graphene-based catalysts towards ORR from the point view of onset potential and electron transfer number. Additionally, graphene samples with different doping levels were also evaluated as catalysts for ORR (Fig. S9, EIS). It was found that both catalytic activity and selectivity improved with the increase of nitrogen doping level. This clearly demonstrated nitrogen doping is responsible for the high catalytic activity towards ORR.

Furthermore, the durability tests reveal that N-Graphene has a higher stability and more tolerance to the crossover effect compared with the commercial Pt/C catalyst. As shown in Fig. 5a, the cyclic voltammograms of N-Graphene did not show a significant change in shape and area after 5000 cycles, which is in contrast to the loss of the active surface area for a commercial Pt/C catalyst (Fig. 5b). The high stability of the N-Graphene can be attributed to the strong covalent bonds between the active sites and the graphitic lattice.[13] Additionally, methanol (a typical fuel for fuel cell) was introduced into the oxygen saturated KOH electrolyte to examine the resistance of N-Graphene to the possible crossover effects. As presented in Fig. 5c, the cyclic voltammograms of N-Graphene in the presence of 3M methanol did not change significantly, indicating that methanol did not interfere with the ORR on the surface of N-Graphene. However, oxidation of the methanol occurred on the surface of Pt/C (Fig. 5d), which could compromise the fuel

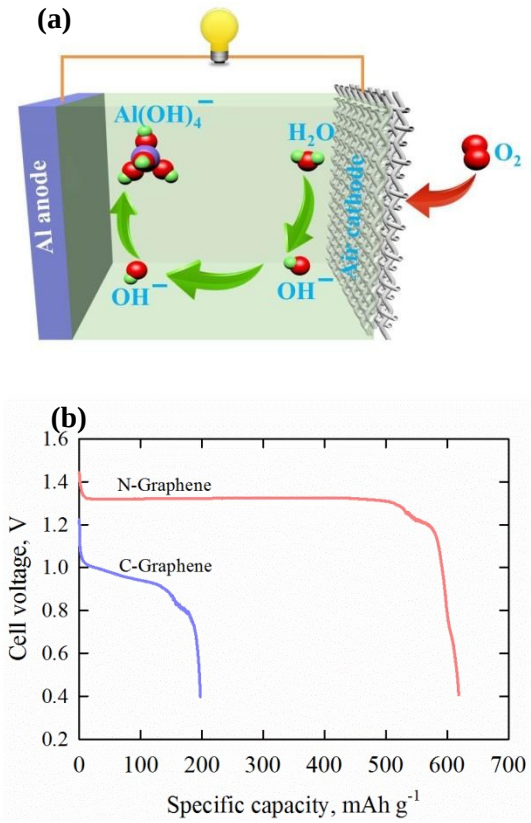

Fig. 6 Schematic illustration of the structure of an Al-air battery (a). Galvanostatic discharge curves of Al-air battery with C-Graphene and N-Graphene as cathode catalysts at a current density of 1 mA cm^{-2} (b). The specific capacity was normalized to the mass of consumed Al.

cell efficiency significantly. Therefore, N-Graphene shows better durability and more tolerance to the crossover effect than Pt/C.

The active sites and the catalytic mechanism of nitrogen-doped graphene towards ORR have been extensively studied but still remain controversial.[7,47] Both quantum mechanical simulations[48] and experimental investigations[49] indicate that pyridinic and/or graphitic nitrogen play an essential role in the ORR process. However, the state-of-the-art investigations tend to support that pyridinic nitrogen is the active sites towards ORR. Recently, Xing and coworkers demonstrated that pyridinic nitrogen are the main active sites for ORR, based on the fact that the ORR intermediate OH(ads) remains on the carbon atoms neighboring pyridinic nitrogen after ORR.[7] Chen and coworkers reported that a higher pyridinic nitrogen concentration gives a better ORR activity.[46] Yasuda and coworkers also revealed that the pyridinic nitrogen reduces oxygen through a four electron pathway, whereas the graphitic nitrogen reduces oxygen through a two electron process.[50] The pyridinic nitrogen is 40-50 at% for nitrogen-doped graphene obtained through this electrochemical exfoliation method (Fig. 2f), which demonstrates the advantages of this novel method and explains well the superior ORR performance of N-Graphene.

Al-air battery

The excellent catalytic performances of N-Graphene towards ORR prompt us to further employ it as cathode catalyst for Al-air battery. Al-air battery is a primary cell, which comprises an Al anode and an air cathode in contact with an aqueous alkaline electrolyte (Fig. 6a). In addition to its extremely high specific energy (8100 Wh kg^{-1}), the high current densities attainable with the Al alloys also make Al-air battery possible for high power density applications.[51,52] The geological abundance of Al metal, a recyclable reaction of aluminium hydroxide, and rapid mechanical rechargeability are additional benefits for Al-air battery.[51,52] During discharge, oxygen is reduced at the air cathode to produce hydroxide ion, which is then transferred across the electrolyte and reacted with the Al anode to form aluminate ion.[51,52] The air cathode is not only one of the most expensive components for Al-air battery but also largely responsible for the cell performance.[51] Metal-based catalysts have been widely employed for air cathode in previous work, such as manganese oxide[53,54] and platinum.[51] To the best of our knowledge, there is no report on nitrogen-doped graphene cathode catalyst for Al-air battery so far.

A home-made Al-air battery was assembled by utilizing N-Graphene and C-Graphene as cathode catalyst. Fig. 6b shows the typical discharge voltage profile of the cell at a constant current density of 1 mA cm^{-2}. The cell with N-Graphene as cathode catalyst exhibits an open circuit voltage of 1.45 V, a well-defined discharge voltage plateau of 1.32 V and a discharge specific capacity of 619 mAh g_{Al}^{-1}. Accordingly, the specific energy of this N-Graphene based Al-air battery reaches up to 817 Wh kg_{Al}^{-1}. These values are even higher than those of Al-air batteries which use metal oxide-based catalysts, such as manganese oxide (437 mAh g_{Al}^{-1} and 528 Wh kg_{Al}^{-1})[53] and $LiMn_2O_4$ (585 mAh g_{Al}^{-1} and 672 Wh kg_{Al}^{-1})[54]. Additionally, it also shows a similar discharge voltage plateau as an Al-air battery which employed nitrogen-doped porous carbon derived from tapioca as cathode catalyst.[56] However, the Al-air battery based on C-Graphene only exhibits an open-circuit voltage of 1.23 V and without obvious discharge voltage plateau. Additionally, the Al-air battery based on C-Graphene only delivers a low discharge specific capacity of 197 mAh g_{Al}^{-1}. The significant difference in the cell performances can be attributed to the high ORR activities of N-Graphene in terms of positive onset potential and large reduction current density, which enable immediate consumption of electrons transferred form the Al anode and thus result in an outstanding performance in the Al-air battery.

Conclusions

In summary, a one-step electrochemical method for the production of nitrogen-doped graphene with tunable nitrogen contents and bonding configurations is developed in this work. Various analyses including AFM, TEM, XPS, Raman, and FTIR indicate the direct formation of high-quality nitrogen-doped graphene from electrochemical exfoliation of graphite in a mixed aqueous electrolyte containing $NH_3 \bullet H_2O$ and $(NH_4)_2SO_4$. The mechanism of nitrogen doping is also proposed, based on analysis of the gas released from graphite electrode during

exfoliation, partially exfoliated graphite and graphene obtained. It is found the introduction of $NH_3 \bullet H_2O$ into the electrolyte is essential for the successful synthesis of nitrogen-doped graphene because NH_3 can be adsorbed on the graphite surface during electrochemical oxidation. This green, efficient, low cost and scalable method provides a possible way for the fast synthesis of high-quality nitrogen-doped graphene which can facilitate the fundamental study of doped graphene and also supplies a promising way for the large scale production of high-quality nitrogen-doped graphene. Additionally, this method is expected to be extended for the electrochemical production of other heteroatom doped graphene by utilizing the same strategy. Furthermore, nitrogen-doped graphene obtained exhibits excellent electrocatalytic activity towards ORR. It is among the best nitrogen-doped graphene-based catalysts for ORR, although the preparation process is extremely facile. Significantly, Al-air battery was assembled by utilizing nitrogen-doped graphene obtained as cathode catalyst for the first time. It shows comparable or even better performances compared with metal-based catalysts.

Acknowledgements

The Research Council of Norway is acknowledged for the support to NTNU NanoLab through the Norwegian Micro- and Nano-Fabrication Facility, NorFab (197411/V30). Support through the FREECATS project funded by the European Union 7th Framework Programme (FP7) is acknowledged.

Notes and references

1 Y. Zhu, S. Murali, W. Cai, X. Li, J. W. Suk, J. R. Potts and R. S. Ruoff, *Adv. Mater.*, 2010, **22**, 3906.
2 A. K. Geim and K. S. Novoselov, *Nat. Mater.*, 2007, **6**, 183.
3 K. S. Novoselov, A. K. Geim, S. V. Morozov, D. Jiang, Y. Zhang, S. V. Dubonos, I. V. Grigorieva and A. A. Firsov, *Science*, 2004, **306**, 666.
4 L. Qu, Y. Liu, J.-B. Baek and L. Dai, *ACS Nano*, 2010, **4**, 1321.
5 P. Chen, T.-Y. Xiao, Y.-H. Qian, S.-S. Li and S.-H. Yu, *Adv. Mater.*, 2013, **25**, 3192.
6 H. Fei, R. Ye, G. Ye, Y. Gong, Z. Peng, X. Fan, E. L. G. Samuel, P. M. Ajayan and J. M. Tour, *ACS Nano*, 2014, **8**, 10837.
7 T. Xing, Y. Zheng, L. H. Li, B. C. C. Cowie, D. Gunzelmann, S. Z. Qiao, S. Huang and Y. Chen, *ACS Nano*, 2014, **8**, 6856.
8 H. Wang, T. Maiyalagan and X. Wang, *ACS Catalysis*, 2012, **2**, 781.
9 H.-W. Liang, X. Zhuang, S. Brüller, X. Feng and K. Müllen, *Nat. Commun.*, 2014, **5**, 1.
10 X.-K. Kong, C.-L. Chen and Q.-W. Chen, *Chem. Soc. Rev.*, 2014, **43**, 2841.
11 C. Huang, C. Li and G. Shi, *Energy Environ. Sci.,* 2012, **5**, 8848.
12 Y. Wang, Y. Shao, D. W. Matson, J. Li and Y. Lin, *ACS Nano*, 2010, **4**, 1790.
13 Z. Lin, G. Waller, Y. Liu, M. Liu and C.-P. Wong, *Adv. Energy Mater.*, 2012, **2**, 884.
14 H. M. Jeong, J. W. Lee, W. H. Shin, Y. J. Choi, H. J. Shin, J. K. Kang and J. W. Choi, *Nano Lett.*, 2011, **11**, 2472.
15 F.-X. Ma, J. Wang, F.-B. Wang and X.-H. Xia, *Chem. Commun.*, 2015, **51**, 1198.
16 G. Wang, L.-T. Jia, Y. Zhu, B. Hou, D.-B. Li and Y.-H. Sun, *RSC Advances*, 2012, **2**, 11249.
17 K. S. Subrahmanyam, L. S. Panchakarla, A. Govindaraj and C. N. R. Rao, *J. Phys. Chem. C*, 2009, **113**, 4257.
18 D. Deng, X. Pan, L. Yu, Y. Cui, Y. Jiang, J. Qi, W.-X. Li, Q. Fu, X. Ma, Q. Xue, G. Sun and X. Bao, *Chem. Mater.*, 2011, **23**, 1188.
19 W. S. Hummers and R. E. Offeman, *J. Am. Chem. Soc.*, 1958, **80**, 1339.
20 C.-Y. Su, A.-Y. Lu, Y. Xu, F.-R. Chen, A. N. Khlobystov and L.-J. Li, *ACS Nano*, 2011, **5**, 2332.
21 K. Parvez, Z.-S. Wu, R. Li, X. Liu, R. Graf, X. Feng and K. Müllen, *J. Am. Chem. Soc.*, 2014, **136**, 6083.
22 R. Gondosiswanto, X. Lu and C. Zhao, *Aust. J. Chem.*, 2015, **68**, 830.
23 X. Lu and C. Zhao, *PCCP*, 2013, **15**, 20005.
24 W.-G. Weng, G.-H. Chen, D.-J. Wu, Z.-Y. Lin and W.-L. Yan, *Synth. Met.*, 2003, **139**, 221.
25 N. R. Wilson, P. A. Pandey, R. Beanland, R. J. Young, I. A. Kinloch, L. Gong, Z. Liu, K. Suenaga, J. P. Rourke, S. J. York and J. Sloan, *ACS Nano*, 2009, **3**, 2547.
26 Y. Zhang, Z. Sun, H. Wang, Y. Wang, M. Liang and S. Xue, *RSC Advances*, 2015, **5**, 10430.
27 L. Zhao, R. He, K. T. Rim, T. Schiros, K. S. Kim, H. Zhou, C. Gutiérrez, S. P. Chockalingam, C. J. Arguello, L. Pálová, D. Nordlund, M. S. Hybertsen, D. R. Reichman, T. F. Heinz, P. Kim, A. Pinczuk, G. W. Flynn and A. N. Pasupathy, *Science*, 2011, **333**, 999.
28 D. Geng, S. Yang, Y. Zhang, J. Yang, J. Liu, R. Li, T.-K. Sham, X. Sun, S. Ye and S. Knights, *Appl. Surf. Sci.*, 2011, **257**, 9193.
29 D. C. Higgins, M. A. Hoque, F. Hassan, J.-Y. Choi, B. Kim and Z. Chen, *ACS Catalysis*, 2014, **4**, 2734.
30 K.-W. Kim, Y.-J. Kim, I.-T. Kim, G.-I. Park and E.-H. Lee, *Electrochim. Acta*, 2005, **50**, 4356.
31 L. Candido and J. A. C. P. Gomes, *Mater. Chem. Phys.*, 2011, **129**, 1146.
32 A. Kapałka, S. Fierro, Z. Frontistis, A. Katsaounis, S. Neodo, O. Frey, N. de Rooij, K. M. Udert and C. Comninellis, *Electrochim. Acta*, 2011, **56**, 1361.
33 H. Gerischer and A. Mauerer, *J. Electroanal. Chem. Interfacial Electrochem.*, 1970, **25**, 421.
34 T. L. Lomocso and E. A. Baranova, *Electrochim. Acta*, 2011, **56**, 8551.
35 K. S. Rao, J. Senthilnathan, Y.-F. Liu and M. Yoshimura, *Sci. Rep.*, 2014, **4**, 1.
36 W. L. Beuschlein and L. O. Simenson, *J. Am. Chem. Soc.*, 1940, **62**, 610.
37 D. Long, W. Li, L. Ling, J. Miyawaki, I. Mochida and S.-H. Yoon, *Langmuir*, 2010, **26**, 16096.
38 J.-H. Zhou, Z.-J. Sui, J. Zhu, P. Li, D. Chen, Y.-C. Dai and W.-K. Yuan, *Carbon*, 2007, **45**, 785.
39 U. Zielke, K. J. Hüttinger and W. P. Hoffman, *Carbon*, 1996, **34**, 983.
40 J. Lu, J.-x. Yang, J. Wang, A. Lim, S. Wang and K. P. Loh, *ACS Nano*, 2009, **3**, 2367.
41 K. Parvez, R. Li, S. R. Puniredd, Y. Hernandez, F. Hinkel, S. Wang, X. Feng and K. Müllen, *ACS Nano*, 2013, **7**, 3598.
42 N. J. Bunce and D. Bejan, *Electrochim. Acta*, 2011, **56**, 8085.
43 X. Li, H. Wang, J. T. Robinson, H. Sanchez, G. Diankov and H. Dai, *J. Am. Chem. Soc.*, 2009, **131**, 15939.
44 Z. Fan, Y. Li, X. Li, L. Fan, S. Zhou, D. Fang and S. Yang, *Carbon*, 2014, **70**, 149.
45 M. Favaro, L. Ferrighi, G. Fazio, L. Colazzo, C. Di Valentin, C. Durante, F. Sedona, A. Gennaro, S. Agnoli and G. Granozzi, *ACS Catal.*, 2014, **5**, 129.
46 Y. Ito, H. J. Qiu, T. Fujita, Y. Tanabe, K. Tanigaki and M. Chen, *Adv. Mater.*, 2014, **26**, 4145.
47 K. Parvez, S. Yang, Y. Hernandez, A. Winter, A. Turchanin, X. Feng and K. Müllen, *ACS Nano*, 2012, **6**, 9541.
48 H. Kim, K. Lee, S. I. Woo and Y. Jung, *PCCP*, 2011, **13**, 17505.

49 L. Lai, J. R. Potts, D. Zhan, L. Wang, C. K. Poh, C. Tang, H. Gong, Z. Shen, J. Lin and R. S. Ruoff, *Energy Environ. Sci.*, 2012, **5**, 7936.
50 S. Yasuda, L. Yu, J. Kim and K. Murakoshi, *Chem. Commun.*, 2013, **49**, 9627.
51 D. R. Egan, C. Ponce de León, R. J. K. Wood, R. L. Jones, K. R. Stokes and F. C. Walsh, *J. Power Sources*, 2013, **236**, 293.
52 M. A. Rahman, X. Wang and C. Wen, *J. Electrochem. Soc.*, 2013, **160**, A1759.
53 F. Cheng, J. Shen, W. Ji, Z. Tao and J. Chen, *ACS Appl. Mater. Interfaces*, 2009, **1**, 460.
54 Y. Liu, J. Li, W. Li, Y. Li, Q. Chen and Y. Liu, *Int. J. Hydrogen Energy*, 2015, **40**, 9225.
55 J. Duan, S. Chen, S. Dai and S. Z. Qiao, *Adv. Funct. Mater.*, 2014, **24**, 2072.
56 M. Wang, Y. Lai, J. Fang, J. Li, F. Qin, K. Zhang and H. Lu, Int. J. Hydrogen Energy, DOI: http://dx.doi.org/10.1016/j.ijhydene.2015.09.054.

Table of contents entry:

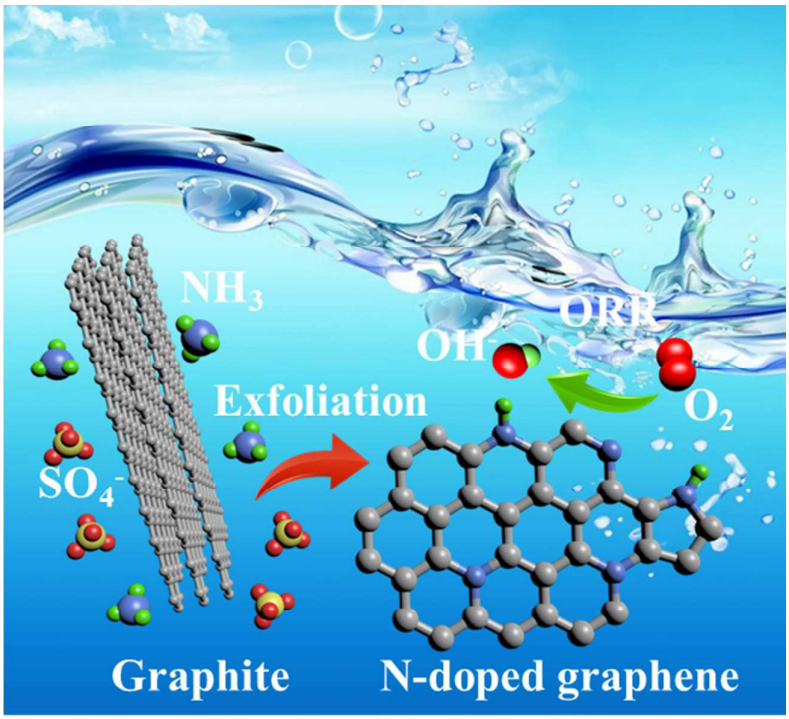

Nitrogen-doped graphene is synthesized by one-step electrochemical exfoliation of graphite, which exhibits superior catalytic performances towards oxygen reduction reaction.